

# FLYEYE TELESCOPE: DESIGN UPGRADE AND DEVELOPMENT STATUS

Piero Gregori<sup>(1)</sup>, Roberta Pellegrini<sup>(2)</sup>, Francesco Cerutti<sup>(3)</sup>, Ernesto Doelling<sup>(4)</sup>, Bernd Sierk<sup>(5)</sup>, Robert Daddato<sup>(6)</sup>, Luca Conversi<sup>(7)</sup>

- <sup>(1)</sup> OHB Italia SpA, via Gallarate 150, 20151 Milano (Italia), Email: [piero.gregori@ohb-italia.it](mailto:piero.gregori@ohb-italia.it)  
<sup>(2)</sup> OHB Italia SpA, via Gallarate 150, 20151 Milano (Italia), Email: [roberta.pellegrini@ohb-italia.it](mailto:roberta.pellegrini@ohb-italia.it)  
<sup>(3)</sup> OHB Italia SpA, via Gallarate 150, 20151 Milano (Italia), Email: [francesco.cerutti@ohb-italia.it](mailto:francesco.cerutti@ohb-italia.it)  
<sup>(4)</sup> ESA/ESOC, Robert-Bosch-Str. 5, 64293 Darmstadt (Germany), Email: [Ernesto.Doelling@esa.int](mailto:Ernesto.Doelling@esa.int)  
<sup>(5)</sup> ESA/ESOC, Robert-Bosch-Str. 5, 64293 Darmstadt (Germany), Email: [Bernd.Sierk@esa.int](mailto:Bernd.Sierk@esa.int)  
<sup>(6)</sup> ESA/ESOC, Robert-Bosch-Str. 5, 64293 Darmstadt (Germany), Email: [Robert.Daddato@esa.int](mailto:Robert.Daddato@esa.int)  
<sup>(7)</sup> ESRIN, Largo Galileo Galilei 1, 00044 Frascati (Italy), Email: [Luca.Conversi@esa.int](mailto:Luca.Conversi@esa.int)

## ABSTRACT

The deployment of ESA's NEO Survey Telescope, the so-called Flyeye telescope, based on innovative technology conceived by OHB-Italia, is in progress. The Flyeye Equatorial Mount has successfully passed all the in-factory verifications and has been upgraded during 2021. Moreover during 2021 the Flyeye Telescope has been further improved in terms of opto-mechanical design and performance optimization.

In 2022 the first phase of the Flyeye program has been nearly completed, with the Flyeye Telescope accepted in-factory.

In the first half of 2023, as output of the in-factory acceptance, the Flyeye cameras will be upgraded installing getter pump to improve their vacuum performance.

An intermediate commissioning and science verification campaign is foreseen to take place within 2023 to integrate the Optics with the Mount and fully verify the Flyeye optical performance at the ASI Space Geodesy Center located in Matera (Italy) waiting for the final installation at the observation site under development by ESA.

## 1 INTRODUCTION

The Near-Earth Object Survey Telescope (NEOSTEL) is an innovative project of the NEO segment of the ESA's Space Safety programme and will in particular focus on the survey and tracking of Near-Earth Objects (NEOs). It will represent the core optical sensor of the NEO-S2P ground based optical observation network.



Figure 1. Flyeye Telescope, the bug-eyed asteroid hunter

NEOSTEL, based on the Flyeye concept, will allow a wide survey strategy, which consists in scanning half of the visible night sky with 4 revisits per field to detect NEO objects characterized by apparent magnitudes down to 21.5. NEOSTEL shall also allow the detection of fast approaching NEO objects, moving at apparent speeds up to 5 arcsec/min. NEOSTEL shall also be able to perform all required follow-up activities, necessary for catalogue maintenance and upgrading, impact monitoring, alert and mitigation, etc.

The NEOSTEL telescope, nicknamed 'Flyeye', splits the image into 16 smaller sub-images to expand the field of view, similar to the technique exploited by a fly's compound eye. Such fly-eyed survey telescopes provide a very large field of view:  $6.7^\circ \times 6.7^\circ$  or about 45 square degrees.  $6.7^\circ$  is about 13 times the diameter of the Moon as seen from the Earth (roughly 0.5 degrees).

The resulting one-meter aperture equivalent telescope is characterized by a two-meter effective focal length, giving rise to a relatively fast optics ( $F/\# = 2$ ). To guarantee the possibility of accurate astrometry, the resolution of the camera must be comparable to the seeing. A pixel size of  $15 \mu\text{m}$ , corresponding to a pixel scale of approx. 1.5 arcseconds, is the best selected compromise for the Flyeye architecture. Following the Flyeye concept application, the optical design of the telescope indicates the possibility to achieve the needed pixel resolution over the required  $6.7^\circ \times 6.7^\circ$  FoV as well as over the entire  $0.47 \mu\text{m} \div 0.78 \mu\text{m}$  spectral range.

The telescope architecture results in a very compact and relatively light structure, which allows fast and precise motion and positioning.

The possibility to support both the follow-up and survey applications allows an efficient percentage of use of the instrument in view of the need to observe at different times during the night depending on the orbital zone of interest.

The Flyeye telescope has the potential of filling a gap in the present scenario of NEO discovery. From an observational point of view the requirement of completing the NEO catalogue calls for pushing as far as possible the limiting magnitude, still keeping a

reasonable large FoV, needed for performing moving object detection. The U.S. optical assets cover the NEO cataloguing need for big and medium size and in the near future deployment and operation of LLST/Vera Rubin Observatory will further push forward the NEO discovery rate. Yet focussing on the small-size tail of the NEO distribution i.e. the Tunguska-size objects (tens of meters), which represent the most likely next major event to actually happen, needs a different approach.

Because of the small size these objects are extremely faint and therefore they can be observed only when they are passing close to our planet and for a very short time. For planetary defence this means being able to cover the whole night sky as efficiently as possible and with a sensitivity high enough to allow sufficient warning time. The technical characteristics of the Flyeye telescope respond at best to setting up an extremely efficient wide-field high-sensitivity network devoted to the detection of potential “imminent impactors” with sufficient warning time. Thanks to the peculiar Flyeye design, highly complementary with respect to the U.S. surveys, the telescope has been selected by ESA for building up its own NEO survey.

## 2 FLYEYE ARCHITECTURE

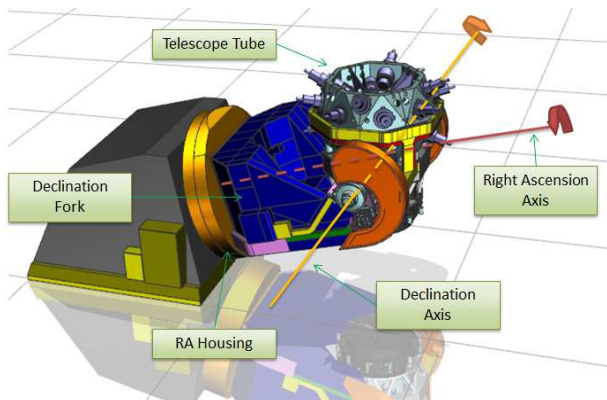


Figure 2. Flyeye Telescope architecture

The telescope consists of the following components:

- a 1 meter aperture class spherical primary mirror provided with a suitable opto-mechanical off-loading cradle based on astatic levers.



Figure 3. Flyeye primary mirror cradle

- A secondary structure hosting the Flyeye optical

core, that is mainly composed of a central beam splitter and sixteen aspherical lenses constituting the so called Beam Shaper as well as sixteen relay optics (Secondary Optical Tubes) distributed all around the secondary assembly itself to realize the tessellation corresponding to the Flyeye wide field of view.

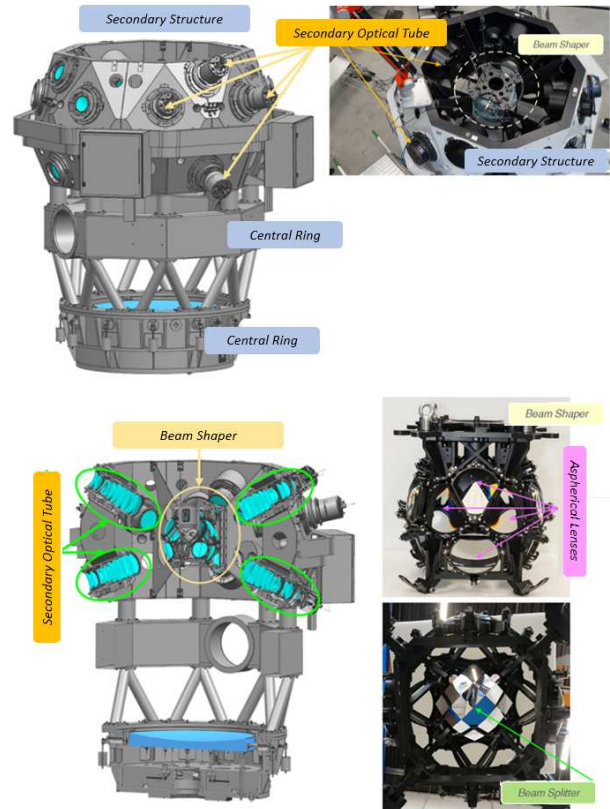


Figure 4. Flyeye main components

In particular, the central beam splitter distributes the incoming light beam into 16 identical optical channels, each of which consists of an aspherical lens, an optical tube, and a focal plane (camera with CCD sensor).

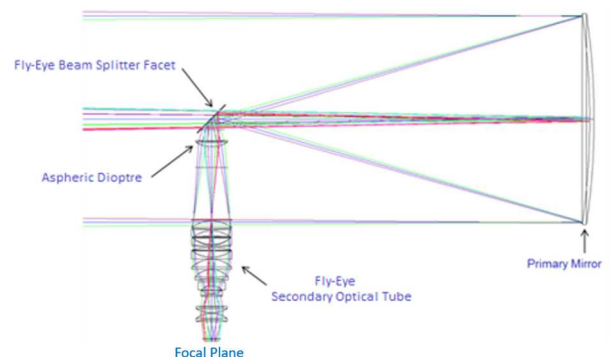


Figure 5. Flyeye channel optical scheme

The secondary optical tubes are necessary to

correct the wave front generated by the primary mirror at the beam shaper exit, up to the required optical resolution, in order to produce the sub-images of the total observed FoV ( $6.7^\circ \times 6.7^\circ$ ) in the individual Focal Planes, where suitable CCD image-recording elements are placed.



Figure 6. Flyeye overview

- Sixteen astronomical CCD cameras: each sensor is an astronomic grade CCD by e2v Teledyne (model CCD231-84-BI) and is operated at  $-45^\circ\text{C}$  by means of a suitable cooling based on a Thermoelectric Cooler (TEC). To allow the maintenance of the operational temperature level, avoid frost on the CCD sensor surface and limit heat exchange, the CCD sensor is located in a vacuum chamber, sealed and kept in vacuum without active pumping. To extract the dissipated heat, the hot side of the TEC is in contact with a heat exchanger connected to a chilled fluid circuit.

OHB-I CCD Camera (ASTROCAD) characteristics	
Resolution	4096 pixels x 4112 pixels
Pixel size	$15\ \mu\text{m} \times 15\ \mu\text{m}$
Image area	$61.44\ \text{mm} \times 61.44\ \text{mm}$
Quantum Efficiency (peak)	$> 95\ \%$
Quantum Efficiency (mean)	$> 75\ \%$
File format	FITS

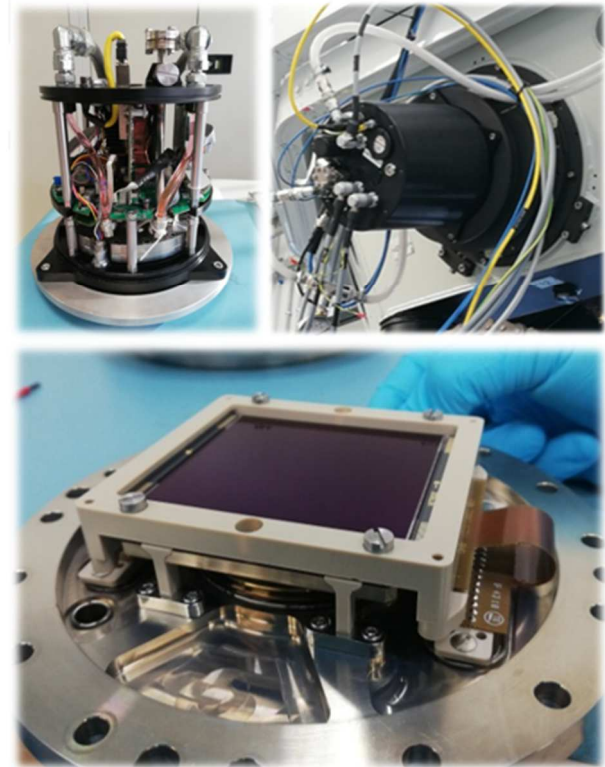


Figure 7. Astronomical CCD Camera (ASTROCAD)

- An equatorial mount that holds the Flyeye telescope orients the direction of view around the right ascension and the declination axis – the celestial coordinates. By doing so, it compensates for the rotation of the Earth by movement of one axis only and avoids image rotation during exposures.

Table 1. Equatorial Mount main features

Fly Eye Equatorial Mount	
Total Weight	$\sim 19\ \text{tons}$
Minimum Pointing over the Horizon	$15^\circ$
Right Ascension Stroke	$\pm 210^\circ$
Declination Stroke	$\pm 75^\circ$
Maximum Speed	$7^\circ/\text{s}$
Maximum Acceleration	$12^\circ/\text{s}^2$
Positioning Accuracy	$\pm 5''$
Tracking Accuracy	$0.3''\ \text{RMS}$



Figure 8. EQM fully integrated during FAT

### 3 FLYEYE IMPROVEMENT

The manufacturing of all the Flyeye telescope components was completed in 2021 according to the initially planned architecture and design described in section 2 of this paper.

In the same year, the telescope was fully assembled at OHB-I's facility in Turate (near Milan), and a preliminary alignment and performance verification campaign was initiated firstly with the aim of preparing the in-factory system acceptance campaign.

An intense activity of integration, alignment and verification has been carried out from the first months of 2020 until the beginning of March 2021. The aim of that campaign was to assess a proper alignment procedure and to have an early verification of the Telescope performance.

During that period several criticalities were experienced, most of them due to the test environment, the seeing limitations at the Turate facility and the absence of the EQM (i.e., no sidereal tracking).

Anyhow, the experience gained during the campaign made it possible to identify some important improvements to be implemented before installing the telescope on the observing site and to identify a better alignment approach.

Following the energy spread study analysis and relevant test sessions carried out in Turate, it has been acknowledged the necessity to develop new OGSEs based on the autocollimation principle to reach the required optical alignment target in factory as well as to make available suitable tools for on-site needs.

The lesson learned during the integration and alignment process in Turate brought to the attention the need to design and manufacture a new Beam Splitter 2.0 (BS 2.0) and Aspherical frame to implement some corrective actions to reduce as much as possible the vignetting effect and the central obstruction.

### 3.1 Telescope improvement

During 2021 the Flyeye first prototype was upgraded accordingly to the above-described modifications. The following components modifications were designed and manufactured:

- Enlarged Beam Splitter (BS) to reduce the vignetting on Upper and Lateral channels
- Aspherical Lenses Frame shape modified to mitigate beams obstruction mostly on Upper channels

The Beam Splitter 2.0 is constituted by a prismatic mirror composed by sixteen planar reflecting facets, enlarged in the external sides. The main objectives of the BS upgrade were:

- ✚ Reduction of the Vignetting effect thanks to the enlargement of the external and lateral mirrors
- ✚ Nominal reflectivity recovery. The Beam Splitter 1.0 was manufactured and integrated in 2017 and undergone several cleaning cycles due the environmental dirty combined with a not expected small glue outgassing effect. As consequence the BS surfaces condition/quality should be assumed partially degraded and suitable to be replaced by the new Beam Splitter.
- ✚ Increasing of the thickness of the glass to obtain a better surface flatness
- ✚ New gluing process with structural glue tested in military optical applications to avoid degradation of the mirror optical surface.
- ✚ Allow future easier maintenance.

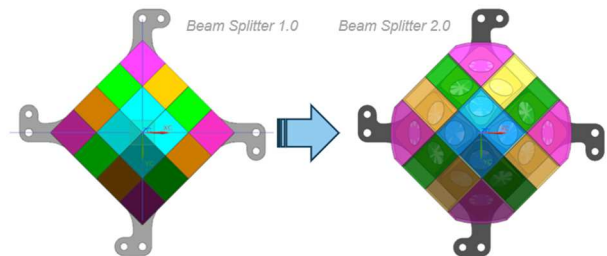


Figure 9. Beam Splitter upgrade

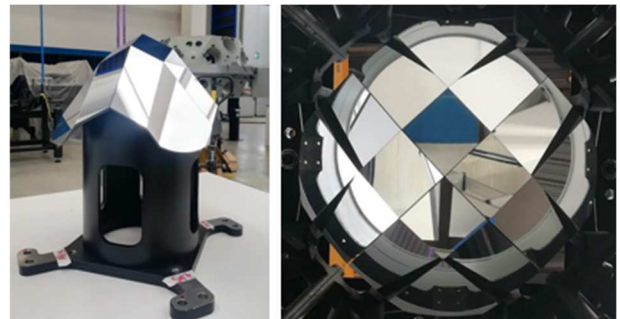


Figure 10. Beam Splitter 2.0

The design upgrade and the construction of a new Aspherical Lenses Frame was completed taking into account the modifications needed to mitigate optical vignetting and beams obstruction mostly on the Upper channels.

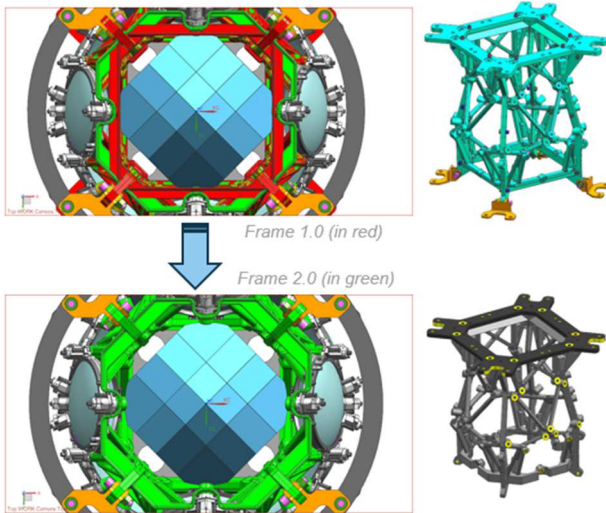


Figure 11. Aspherical Lenses Frame upgrade.

The Upper Channel Ray Tracing images reported below highlights the obstruction affecting the original design and gives evidence of the constraints considered in the redesign of the frame geometry in with the frame bottom side shape was modified from square to octagonal to mitigate the beam interference with the structure.

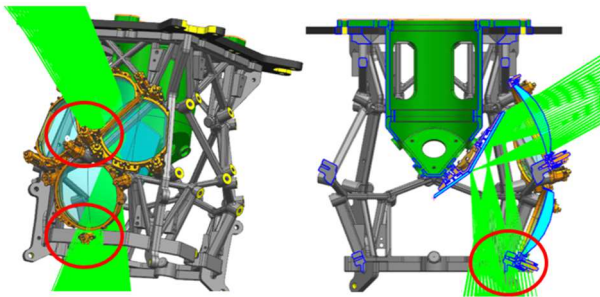


Figure 12. Upper channel obstruction to be solved.



Figure 13. New aspherical lenses frame manufactured to solve mainly the upper channels obstruction.

The comparison of vignetting for the full FoV between original and upgraded (2.0) configurations is presented in the following figure to highlight the achieved improvement.

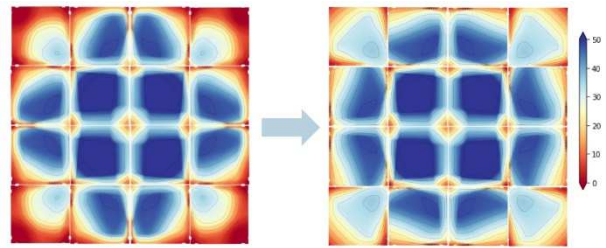


Figure 14. Vignetting map of the original design (left) compared with the one obtained with upgrade 2.0 (right).

### 3.2 Alignment procedure improvement

The indoor pre-alignment procedure based on Newton's rings technique – initially conceived as baseline for the alignment approach – was not suitable to properly identify the SOT axis affecting therefore the optical channel alignment.

A new alignment procedure based on autocollimation principle has been defined in 2021 and new optical ground support equipment (OGSE) manufactured ad hoc to apply this new approach.

The sixteen optical channels must be independently aligned but maintaining the nominal distance in between adjacent channels in order to realize the foreseen channels tessellation meaning, in other words, to compose the mosaic that constitutes the Flyeye 45-square-degree field of view. A mask (Field Tessellation Mask – FTM), placed in between the primary mirror and the beam splitter, is adopted to identify the sixteen nominal reference direction.

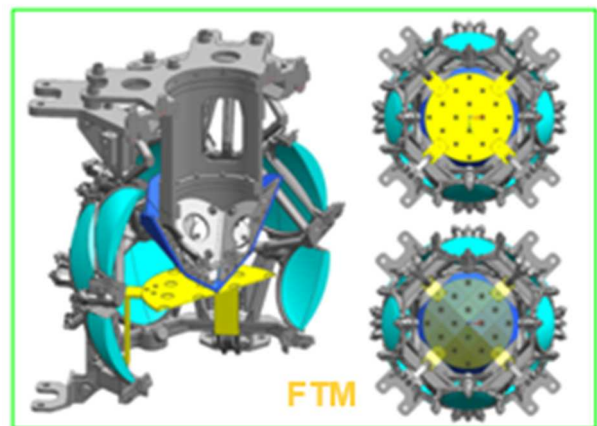


Figure 15. Field Tessellation Mask (FTM)

The autocollimation axis of each channel is identified by a dedicated laser OGSE (Lase Alignment Gauge – LAG) installed on the external side of the optical channel to be aligned.

In synthesis, the alignment procedure consists of serially auto collimating the optical elements along the optical path of each channel according to the sequence below:

1. the reference laser beam (LAG) is auto collimated with the primary mirror according to the direction identified for the channel by the mask mentioned above (FTM)

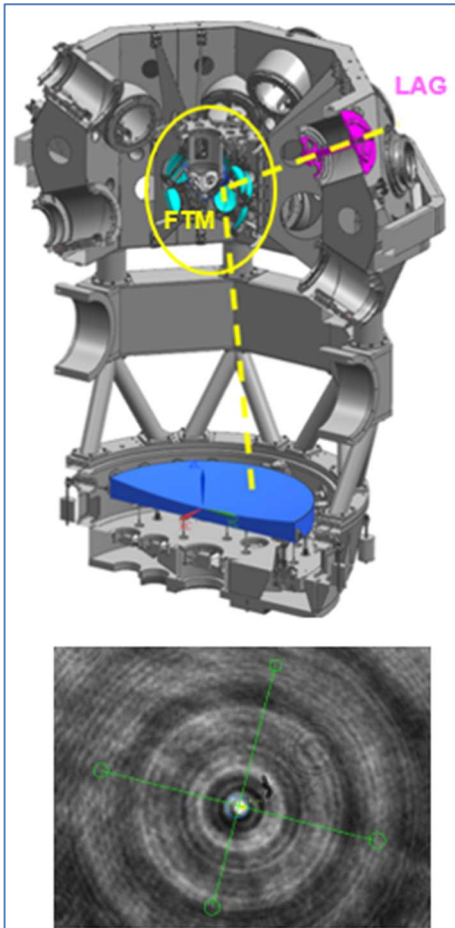


Figure 16. Typical auto collimation configuration for the new Flyeye alignment procedure with detail of the auto collimated overlapped spots

2. the aspherical lens is integrated and auto collimated according to the direction identified in step 1
3. the SOT is integrated and auto collimated with the aspherical lens and the primary mirror by maintaining the reference laser beam passing through the dedicated reticle on the FTM mask
4. the main optical axis of the SOT is identified with a dedicated tool (Secondary Optical Tube Reference Axis - SOTAR) to generate a laser beam that materializes the SOT axis
5. the CCD Camera is integrated and aligned by auto collimated the CCD sensor in according to

the SOT optical axis identified at step 4.

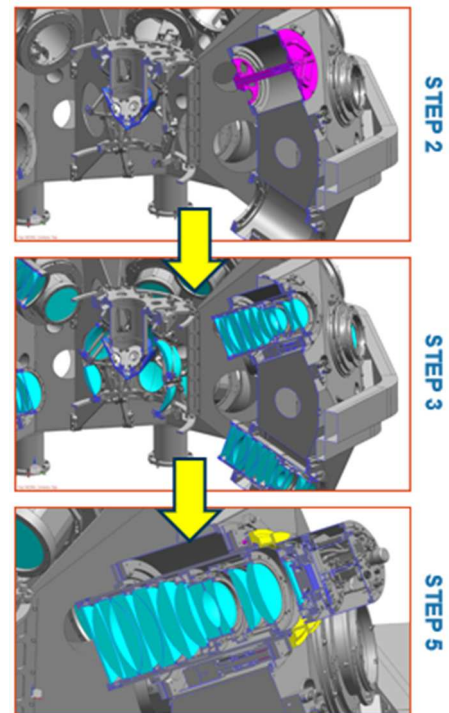


Figure 17. Main auto collimation procedure steps sketch.

The last steps of the Flyeye channel alignment are:

- clocking of the cameras
- the focal planes / optical channels overlapping verification

The clocking of the cameras (i.e. the orientation of each of the sixteen focal plane around its main axis to compose the FoV mosaic with the proper orientation and overlapping between adjacent channels) can be performed in factory using a collimator or by sky observation. In both configuration a trail will be generated on the focal plane, in one case a trail produced by the laser beam spot and in the other by stars trailing. Each camera will be rotated around its main axis (orthogonal to the focal plane) in order to have trails oriented diagonally at 45 degrees.

The channels overlapping can be easily verified during sky observations. Exploiting the capabilities of a plate solving software algorithm (astrometry.net), each pixel can be associated to a specific sky position through an astronomical coordinate system. In this way all the images can be tiled into one to compose a mosaic allowing the estimation of the relative position of each sub-FoV with respect to the others, the total angular portion of the sky observable and the overlapping area of the adjacent cameras / sub-FoVs. This test is also a direct proof of the channels overlap and therefore of the field continuity (sub-FoVs overlapping). The test can be performed with a single synchronous acquisition of all the 16 cameras. If the sidereal tracking is not available (as

in Turate where the Telescope is integrated on a dedicated MGSE instead of on the EQM), all the images must be taken synchronously and with a short exposure time (i.e. 0.5 s) to avoid any positional error due to the relative delay of different channels and to overcome the missing sidereal tracking.

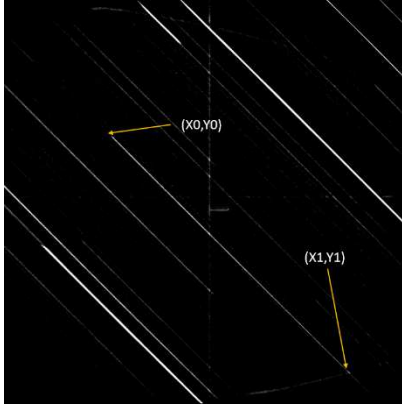


Figure 18. Example of camera clocked by sky observation with stars trailing oriented at 45 degrees.

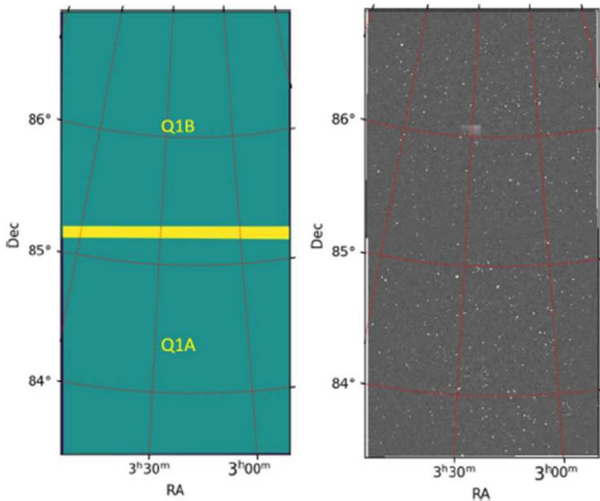


Figure 19. Example of mosaic composition of two adjacent channels for the overlapping and continuity verification.

### 3.3 Equatorial mount improvement

The equatorial mount was integrated and accepted in the second half of 2018 at the manufacturer's facility in Villafranca (Italy).

During the period 2021-2022 the equatorial mount software was upgraded introducing an additional implementation called "forbidden region".

The forbidden region subsystem prevents the equatorial mount from moving below a given elevation angle as there is a risk of breakage of the primary mirror if it is overturned. As a safety measure, three anti-flip

mechanical stops are installed at the edge of the mirror to mitigate problems in case the telescope is pointing below the horizon. Despite these devices, an additional protection needs to be foreseen preventing the telescope to point below a given elevation angle.

Consequently, the EQM software has been updated in order to allow the following movements:

- Maintenance forbidden region (elevation  $< 1^\circ$ ): only manual movement towards higher elevations allowed.
- Intersection of maintenance region and normal operation forbidden region ( $1^\circ \leq \text{elevation} < 15^\circ$ ): no movements are allowed when in positioning, survey, follow-up, sweep and parking modes; in maintenance mode only movements at reduced speed are allowed when moving towards the lower elevations.
- Normal operation region (elevation  $\geq 15^\circ$ ): all movements are allowed.

The "forbidden region" implementation was tested in Villafranca in October 2022 when an EQM delta-FAT occurred. The delta-FAT objective was also to verify the EQM kinematic and pointing performance after the integration on the mount of all cables and pipes needed for the Flyeye. All the additional tests were successfully passed.

## 4 FLYEYE FIRST PROTOTYPE PERFORMANCE SIMULATION

As a starting point for the analysis, Flyeye performances are simulated considering the ideal case of having the telescope in its nominal configuration, without optical distortion due to atmospheric seeing and with perfectly aligned optics and without noise contribution from the sky background. This ideal simulation set-up allows to evaluate the consistency of the telescope optical scheme, providing a representative case for the optical system. In the following table the simulation results for the ideal case is reported. In this simulation, the sky background photon-flux is set to zero.

The full curves of FoV coverage percentage are reported in Figure 4-1, 4-2.

	Exposure Time= 40s	
MAG	SNR Threshold=3	SNR Threshold=4
21	99,38	98,54
21,2	98,86	97,56
21,5	98,02	94,96

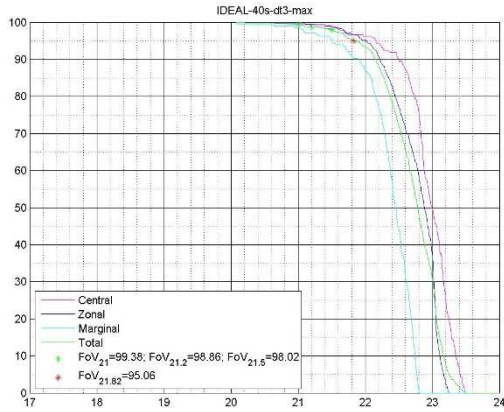


Figure 20. FoV coverage percentage for the ideal case with threshold 3.

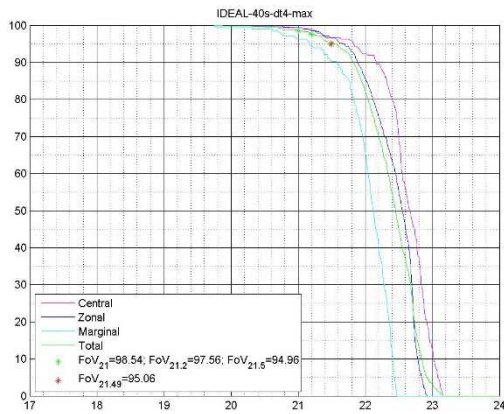


Figure 21. FoV coverage percentage for the ideal case with threshold 4.

The total vignetting map, together with the ensquared energy map in the ideal configuration are shown in the following figures.

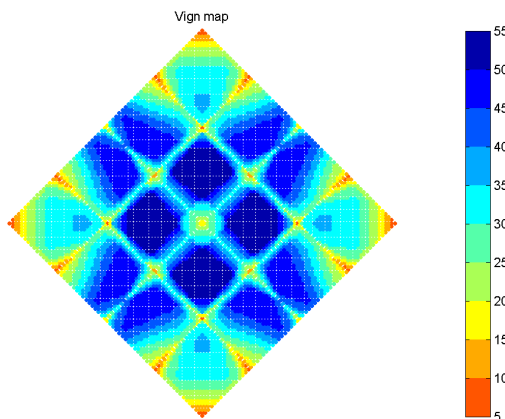


Figure 22. Vignetting map of the entire FoV in the ideal case. The color-map gives the percentage of un-vignetted light.

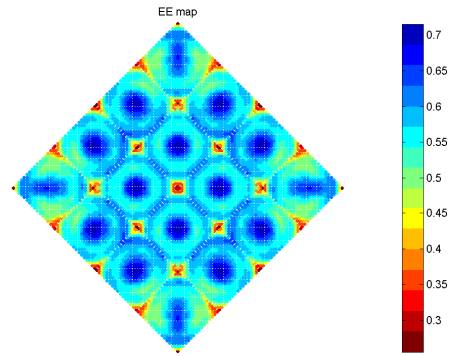


Figure 23. Ensquared energy map in the ideal configuration, exposure time set at 40s.

In order to perform a realistic performance analysis to identify a pass/fail criteria for the performance acceptance at the first foreseen installation site in Matera, several perturbative effects are included in the nominal telescope configuration. First of all, degradation effects induced by the observatory site are added, such as atmospheric seeing and sky-background illumination. The astronomical seeing of the selected site is assumed to be 1.5", while the sky background magnitude is assumed to be 21.0 mag in the V photometric band. Moreover, perturbations in the optical alignment accuracy and manufacturing, as well as perturbations induced by gravity, are included. Such effects give a configuration as realistic as possible.

Monte Carlo (MC) simulations produce the perturbations in the nominal configuration, giving two main cases used in the analysis: a best MC case and a worst one.

#### 4.1 Performance analysis: Methods

Due to the telescope large field of view, the limiting magnitude performances has been analysed first constructing a precise SNR analytical model and then using such a model to precisely compute the SNR value on a large set of angular positions. In particular, the adopted method is the following.

The field of view of each channel is sampled with 481 points. Using Zemax software, both vignetting due to optomechanical design, and the ensquared energy are evaluated at each sample point. The ensquared energy is computed including the atmospheric seeing. Finally, the SNR function is evaluated at each sample point as a function of the source apparent magnitude.

## 4.2 SNR analytical model

As mentioned above, a precise SNR model is required to evaluate the telescope performances in terms of the limiting magnitude. The telescope SNR model depends on different parameters derived from the source photometric properties, as well as from the optical design and noise sources.

For a fixed object, the signal collected by the peak pixel on the CCD sensor depends on the flux coming from the source as “filtered” by the telescope optical components ( $f_{NEO}$ ), the exposure time together with the ensquared energy EE, the telescope aperture A and the vignetting factor. Vignetting depends on both the central obstruction, and on other sources of vignetting. The signal can be expressed as

$$S = f_{NEO} \cdot A \cdot EE \cdot vig \cdot t \quad (1)$$

Figure 2-1 shows the telescope vignetting map, which depend neither on site parameters, such as seeing, nor on exposure time or SNR threshold.

The effect of the optical components of the Flyeye telescope on the received flux can be modelled through the transmission curve of the Flyeye telescope  $T(\lambda)$ . The flux of a NEO object “filtered” by the telescope is computed from the product, over the telescope spectral operational band, of the specific irradiance  $I(\lambda)$  with the telescope overall transmission curve  $T(\lambda)$

$$f_{NEO} = \int_{400\text{ nm}}^{800\text{ nm}} I(\lambda)T(\lambda)d\lambda \quad (2)$$

The transmission curve defines the overall throughput of the telescope, and it depends on different factors such as CCD quantum efficiency, filter transmission and mirrors reflectivity and transparency of the lenses.

The integrated flux from an NEO-like object can be expressed in terms of the object magnitude in the V-band, once the flux of a zero-magnitude NEO  $f_0$  is computed, and the received signal is

$$S = f_0 \cdot 10^{10-0.4mv} \cdot A \cdot vig \cdot EE \cdot t \quad (3)$$

Concerning the noise component of the SNR model, its main contributors are: photon counting uncertainty originating from the observed object photon flux, as well as from the sky background; thermal noise arising from dark current  $D(T)$  effect and read-out noise  $RN$ . Taking into account all these different sources, the total noise

component is given by

$$N = \sqrt{\sigma_{P,D}^2 + RN^2 + \left(\frac{G}{2}\right)^2} \quad (4)$$

Where  $\sigma_{P,D}^2$  collects the total photon counting uncertainty plus the dark current noise, while  $G$  is the camera gain.

$$\sigma_{P,D}^2 = f_{NEO} + (f_{0,bkg} \cdot 10^{10-0.4mv,sky} \cdot A \cdot vig \cdot PS^2 + D) \cdot t \quad (5)$$

The SNR analytic model is then

$$SNR = \frac{f_0 \cdot 10^{10-0.4mv} \cdot A \cdot vig \cdot EE \cdot t}{\sqrt{\sigma_{P,D}^2 + RN^2 + \left(\frac{G}{2}\right)^2}} \quad (6)$$

## 4.3 SIMULATION MC RESULTS FOR MATERA SITE

The telescope performances are summarized comparing the percentage of FoV that meets SNR (FoV coverage percentage in the following), as a function of the object apparent magnitude, in the two aforementioned realistic configurations (i.e. best and worst MC cases). The comparison between the best and worst case is performed varying three main parameters that impact the telescope detection performance: the exposure time, the threshold for detection and the dark current in the CCD considering different operational temperatures ( $-45^\circ\text{C}$  and  $-50^\circ\text{C}$ ). The following tables summarizes all the simulation results.

Table 3. Comparison between best (green) and worst (red) cases at different exposure time and dark current intensity. SNR detection threshold equal to 4.

MAG	SNR Threshold=4							
	Dark Current: 12 @ CCD Temp = -45°C				Dark Current: 6,5 @ CCD Temp = -50°C			
	40s		60s		40s		60s	
21	58.52	35.76	82.59	67	63.51	42.36	87.16	70.84
21.2	24.74	10.03	63.77	42.83	32.22	14.19	69.44	49.95
21.5	2.18	0	18.87	4.68	3.27	0	23.7	8.42

Table 4. Comparison between best (green) and worst (red) cases at different exposure time and dark current intensity. SNR detection threshold equal to 5.

MAG	SNR Threshold=5							
	Dark Current: 12 @ CCD Temp = -45°C				Dark Current: 6,5 @ CCD Temp = -50°C			
	40s		60s		40s		60s	
21	19.23	4.83	58.52	35.71	23.44	8.52	64.14	42.57
21.2	3.64	0	24.53	9.67	5.25	0	32.22	13.77
21.5	0	0	2.08	0	0	0	3.12	0

As illustrative examples, some FoV coverage curves are reported for some representative cases.

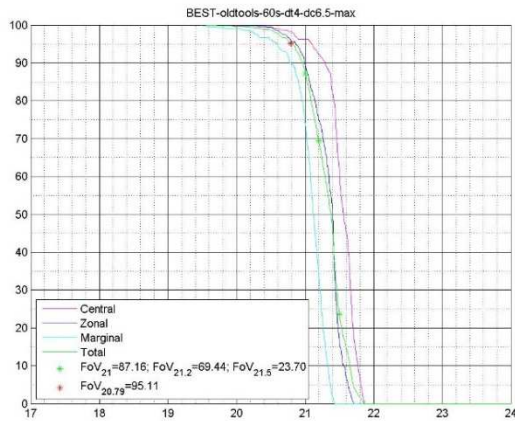


Figure 24. FoV coverage for the best case with 60s of exposure time, SNR threshold of 4 and dark current of 6.5.

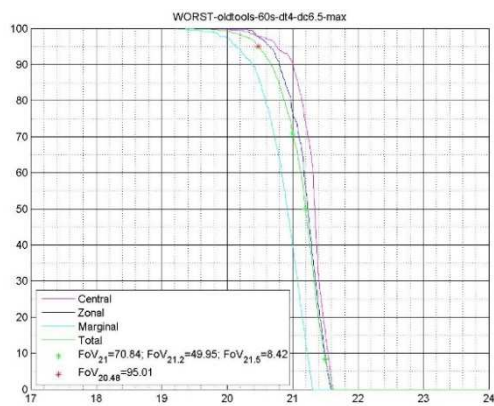


Figure 25. FoV coverage for the worst case with 60s of exposure time, SNR threshold of 4 and dark current of 6.5.

## 5 FLYEYE DEVELOPMENT STATUS

An intense activity of integration, alignment and verification has been carried out from the first months of 2020 until the beginning of March 2021. As described in paragraph 3, that campaign led to the improving of the Flyeye system that has been completed in 2021.

Considering the seeing limitation in Turate and the missing of EQM, it is not possible to verify the performances at telescope stand-alone level.

In the meantime, ASI has launched an initiative which encompasses a broad spectrum of activities. Hosting the first ESA Flyeye telescope at its Space Geodesy Center located in Matera (Italy) for a temporary installation will allow to carry out an extensive testing of its performances for NEO detection in an ideal logistic site and with suitable ambient condition, as well as to figure out the possible applications for space surveillance in a realistic environment.

In 2018, ESA and ASI signed an agreement dedicated to the installation of the first Flyeye telescope on the Italian

national territory on Mount Mufara, in Sicily. But considering the above, ESA and ASI have agreed to proceed with a temporary installation of the Flyeye telescope in Matera.

With the possibility to move in Matera, the ESA Flyeye acceptance test campaign has been modified as reported in the following diagram:



Figure 26. Flyeye acceptance campaign phases

The FAT-1 campaign in Turate has been completed with the objective to verify the Secondary Optical Assembly correct integration/alignment and the System functionality. The FAT-1 has been split in two parts:

- FAT-1A, with the verification of the auto-collimation of all the sixteen optical channels, Sub-FoV phasing and overlapping verification and FoV continuity
- FAT-1B with function and software verification

A mosaic image showing the large Field of View ( $6,7^\circ \times 6,7^\circ$ ) of the Flyeye Telescope is depicted in the figure below; this mosaic is made assembling sixteen images acquired using the CCD cameras during sky observation performed in Turate. Even if atmospheric conditions (atmospheric seeing and sky background) are not suitable for measuring telescope performance, they are still sufficient to make the necessary astrometric reduction that allows each sub-FoV to be assigned the correct portion of the observed sky. An artifact of the moon has been pasted in the mosaic to give evidence of the impressive dimensions of the FoV.

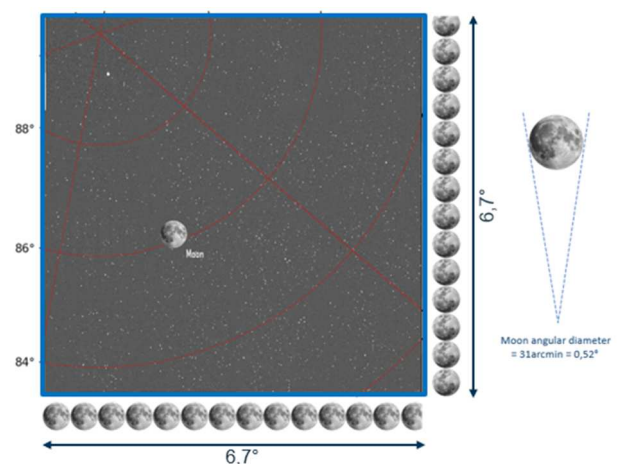


Figure 27. Flyeye mosaic representing the overall FoV

In the following, Flyeye synchronous images footprint is shown to highlight the overlapping areas of the adjacent sub-Field of Views. Also, in this case the overall footprint has been derived from real sky image acquired in Turate to demonstrate the overall FoV continuity.

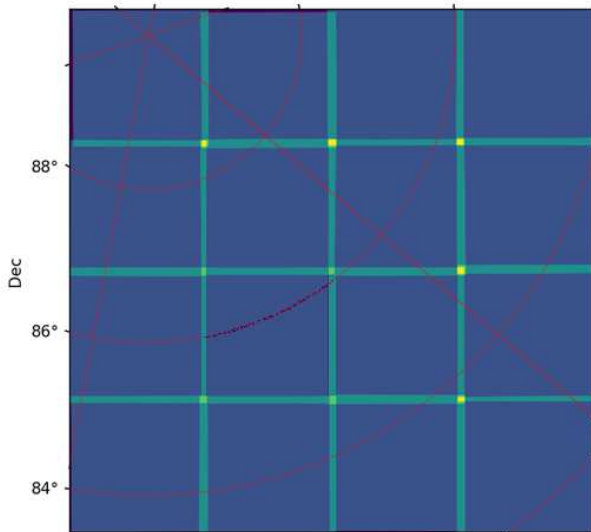


Figure 28. Flyeye overall FoV footprint



Figure 28. Flyeye telescope in Turate waiting for sky night observation.

In conclusion, the FAT-1 campaign has been successfully completed with only a major task to be investigated and solved related to a degraded performance in term of target temperature on some CCD cameras.

## 5.1 Camera investigation and improvement

During the ASTROCAD performance test and mostly the telescope FAT in Turate, some cameras did not reach the target temperature on CCD sensor (operating temperature of the CCD must be less than or equal to  $-45^{\circ}\text{C}$ ) and did not maintain the needed vacuum level for at least six months. As outcome of the FAT-1 performed in Turate, an investigation has been performed in the last months of 2022 to solve the mentioned not compliances.

The required low temperature, needed to obtain the required sensor efficiency in term of dark current value, has been verified to be strictly linked to the vacuum level inside the chamber that hosts the CCD sensor.

The investigation has been completed in December 2022 with the conclusion that the current cameras can comply the acceptance requirements ( $T_{\text{CCD}} \leq -45^{\circ}\text{C}$ ) with a good margin and can reduce the dispersion of thermal characteristics, improving the vacuum performance of the camera.

Maintaining the vacuum level proved to be the most decisive parameter for complying with the thermal specification. This scope will be ensured installing a getter pump, model SAES Capacitorr Z100, could be considered adequate to maintain an optimal vacuum level over time and consequently maintain excellent thermal characteristics. NEG pump reactivation once a year is recommended.



Figure 29. Flyeye Camera in laboratory: getter pump test set up

The Flyeye cameras refurbished with getter pump is foreseen to be available at mid-2023.

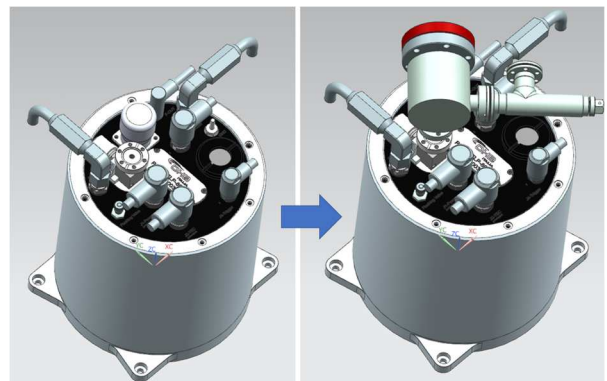


Figure 30. Comparison between camera current model and the upgraded one with getter pump installed.

## 6 FLYEYE PROGRAM: NEXT PHASE

*infrastructure*

As anticipated in the previous paragraph, the next phase will be the FAT-2 to be performed in Matera.

ASI has signed a contract with OHB Italia for the construction of the infrastructure necessary to host this first Flyeye in Matera.

Currently the infrastructure design for Matera installation has been defined and we are waiting for the final permission from Municipality and Region to start the infrastructure construction that is foreseen to be available in the third quart of 2023.

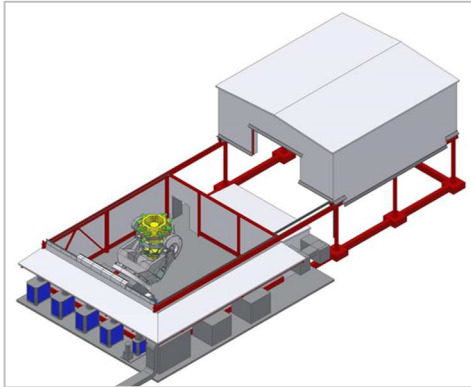


Figure 31. Sketch of the Matera infrastructure

After completion of the Flyeye commissioning and science verification to be performed in Matera, the telescope will be moved to the final site.

The infrastructure for the site foreseen in Monte Mufara, Sicily, is under development directly by ESA, with EIE Group as the prime contractor. In the following picture an overview of the final dome hosting the Flyeye is shown.

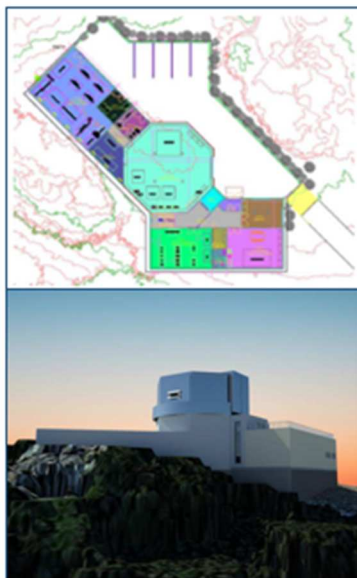


Figure 32. Rendering and sketch of the Monte Mufara

## 7 CONCLUSIONS

The Flyeye team experience gained in recent years from the integration, alignment and on-field testing of Flyeye telescope is a highly valuable heritage. A few key points have been identified both at hardware and procedural level starting from the initial design up to the deployment of an improved prototype. These aspects have led to the definition of an instrument that can be the core optical sensor for Space Safety Programme (S2P), combining a very wide Field of View (FoV), good astronomical resolution and fast repositioning capabilities.

The Flyeye telescope will be able to implement an NEO wide survey strategy, finding unknown dangerous asteroids rushing towards the Earth at least a week in advance.

For Space Surveillance Tracking (SST), its survey observations allow to catalogue objects with a diameter of about 7-10 cm placed in orbit at an altitude of 1000 km (High LEO),

The first Flyeye prototype developed for the European Space Agency (NEO discovery and detection) has been fully aligned in factory and will be transferred to its initial observation site in 2023 for the “first light” on sky.

## 8 REFERENCES

1. Cibin, L., Chiarini, M., Gregori, P., Bernardi, F., Ragazzoni, R., Sessler, G., Kugel, U., (2019). The Flyeye Telescope, Development and First Factory Tests Results. In Proc. - 1<sup>st</sup> NEO and Debris Detection Conference, Darmstadt, Germany.
2. Vellutini, E., Gregori, P., Pellegrini, R., Dimare, L., Bernardi, F., Di Cecco, A., Castronuovo, M.M., Marzo, C., Perozzi, E., (2022). Exploiting the synergies of observing NEO and space debris with the Flyeye telescope. 73rd International Astronautical Congress (IAC), Paris, France.
3. Di Cecco, A. et al., Analysis of Italian sites for NEO and space debris observations with the ESA Flyeye telescope, Proc. of the ESA NEO and Debris detection Conference exploiting synergies, 22-14 January 2019, Darmstadt, Germania, published by ESA Space Debris Office;

Dotto and the NEOROCKS Team. The EU NEO Rapid Observation, Characterization and Key Simulations project. EPSC Abstracts Vol.15 EPSC2021-389, 2021.